TILTING PAD JOURNAL BEARING PIVOT DESIGN FOR HIGH LOAD APPLICATIONS

by

John C. Nicholas

Rotating Machinery Technology, Inc.

Wellsville, New York

and

Karl D. Wygant

Research Assistant

University of Virginia

Department of Mechanical, Aerospace and Nuclear Engineering

Charlottesville, Virginia

John C. Nicholas received his B.S.A.E. degree from the University of Pittsburgh (1968) and his Ph.D. degree from the University of Virginia (1977) in rotor and bearing dynamics. While at Virginia, he authored the tilting pad and pressure dam bearing computer programs that are used by many rotating equipment vendors, users and consultants.

Dr. Nicholas has worked in the turbomachinery industry for the last 18 years in the rotor and bearing dynamics areas, including five years at Ingersoll-Rand and five years as the supervisor of the rotor dynamics group at the Steam Turbine Division of Dresser-Rand.

Currently, Dr. Nicholas is part owner and Chief Engineer for Rotating Machinery Technology Incorporated, a company that repairs turbomachinery and manufactures high performance tilting pad journal and thrust bearings, sleeve bearings and seals for the rotating equipment industry for the last nine years.

Dr. Nicholas, a member of ASME, STLE, and the Vibration Institute, has authored 29 technical papers concerning tilting pad bearing design, pressure dam bearings, rotordynamics, and support stiffness effects on critical speeds.

Karl D. Wygant received a B.S. degree (Mechanical Engineering) from Clarkson University in 1988. From 1988 to 1989, he worked as an analytical engineer in the rotor dynamics group at the Steam Turbine Division of Dresser-Rand. Mr. Wygant received a M.S. degree (Mechanical Engineering) from the University of Virginia (1993). His Master's research dealt with the modification of a rotor-bearing stability code to handle multiple degrees of freedom support/casing models.

Mr. Wygant is currently pursuing a Ph.D. at the University of Virginia. His area of research is the experimental determination of the thermal, static and dynamic properties of tilting pad journal bearings.

ABSTRACT

Reducing pivot stress, pivot wear and preventing pivot failure are major design challenges encountered by tilting pad bearing designers in the extremely high load regime where the bearing unit load may often range up to 500 psi.

In an attempt to address these design challenges, simple equations are presented for the calculation of pivot stiffness and the resulting pivot contact stress for a nonaligning cylindrical pivot, a self-aligning spherical pivot and a self-aligning sphere-in-a-cylinder pivot. The effect of the pivot's flexibility on the bearing's stiffness and damping properties is also investigated. Comparisons are made between the three pivot designs.

Utilizing the simple equations for pivot stress, a method to determine proper pivot sizing to prevent pivot failure due to high loads is outlined using a spherical pivot as a design example. A finite element stress analysis is also considered and the results compared to the simplified analysis.

INTRODUCTION

One of the disadvantages of tilting pad journal bearings is that they introduce additional flexibilities between the bearing oil film and the ground. The tilting pad itself has its own flexibility [1] and the pad pivot is also flexible [2]. These flexibilities reduce the apparent bearing stiffness and decrease the bearing effective damping thereby lowering rotor critical speeds and increasing shaft vibration [3, 4].

For these reasons, it is important to design pad pivots to be as stiff as possible. Furthermore, as the pivot stiffness increases, the pivot stress and thus pivot wear during operation decrease. This is also important as increased clearance from pivot wear may decrease the bearing damping.

Reducing pivot stress, pivot wear and preventing pivot failure are major design challenges encountered by tilting pad bearing designers in the extremely high load regime where the bearing unit load may often range up to 300, 400 or even 500 psi. The problem is exacerbated by the often stipulated requirement that the tilting pad pivot must be self-aligning and capable of adjusting itself to accept several degrees of pad-to-shaft axial misalignment. This type of high load application is most common for high performance gear boxes and integrally geared compressors that produce very large gear forces. In an attempt to address these design challenges, simple equations will be presented for the calculation of pivot stiffness and the resulting pivot stress for a nonaligning cylindrical pivot, a self-aligning spherical pivot and a self-aligning sphere-in-a-cylinder pivot. The effect of the pivot's flexibility on the bearing's stiffness and damping properties will also be investigated. Comparisons will be made between the three pivot designs.

Utilizing the simple equations for pivot stress, a method to determine proper pivot sizing to prevent pivot failure due to high

loads will be outlined using a spherical pivot as a design example. A typical high stress pivot failure is shown in Figures 1, 2, and 3 for a spherical pivot. In Figure 1, the failure starts with a crack in the bronze pad at the bottom of the spherical seat. Next, the pad cracks at its center (Figure 2). Finally, the pad breaks in half as seen in Figure 3. This failure occurred in an actual machine that was undergoing excessively high vibration caused by large unbalance forces. The high vibration imparted high dynamic loads on the pad and pivot causing the pad to crack and eventually break.

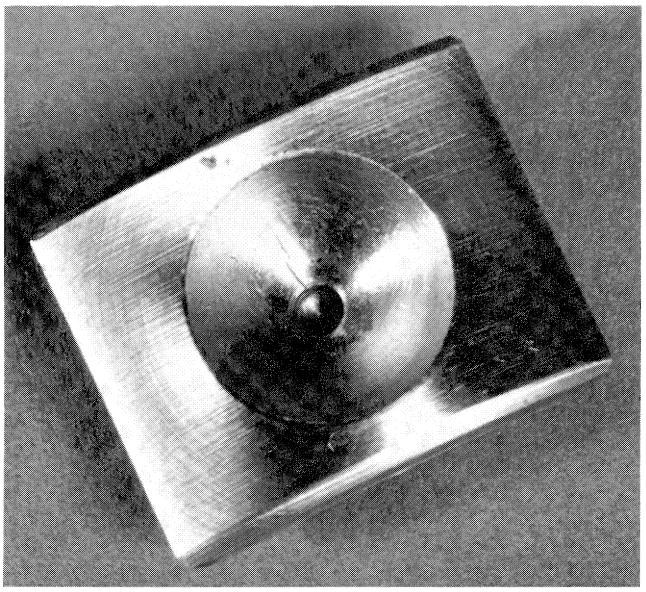

Figure 1. Failed Pivot with Cracked Pivot Seat.

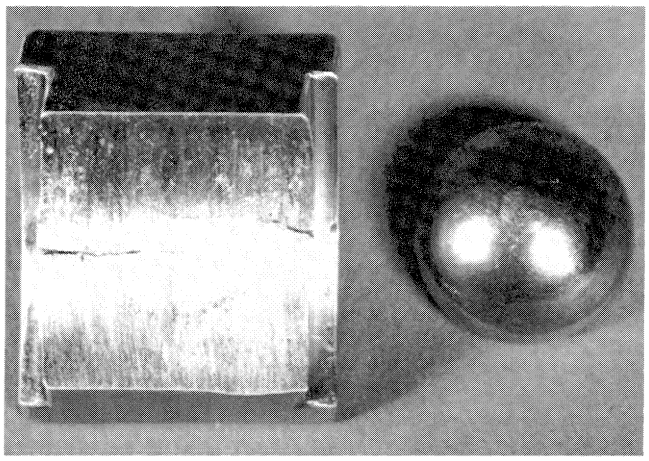

Figure 2. Failed Pivot with Cracked Pad.

A finite element stress analysis will also be considered and the results compared to the simplified stress analysis for an example spherical pivot.

PIVOT STIFFNESS

Spherical Pivot

A self-aligning spherical pivot is depicted in Figures 4 and 5. The steel spherical ball pivot rides in a spherical seat that has been machined into a journal bearing's tilting pad which is

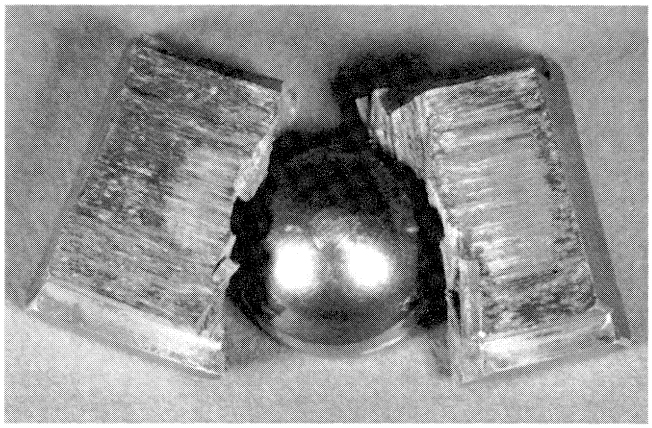

Figure 3. Failed Pivot with Broken Pad.

typically manufactured from bronze. Define the following parameters:

W_p = pivot load, lbs
D_p = pivot diameter, in
D_h = housing or spherical seat diameter, in

Kirk and Reedy [2] defines the pivot stiffness, K_p, as

$$K_p = \frac{\partial W_p}{\partial \delta_p} \quad \text{(lbs/in)} \tag{1}$$

The pivot deflection, δ_p, and stiffness for a spherical pivot are [2,5]

$$\delta_p = (1.040) \cdot \left(\frac{W_p^2 C_2^2}{C_1} \right)^{\frac{1}{3}} \text{(in)} \tag{2}$$

$$K_p = (1.442) \cdot \left(\frac{C_1 W_p}{C_2^2} \right)^{\frac{1}{3}} \tag{3}$$

where

$$C_1 = \frac{D_h D_p}{D_h - D_p} \tag{4}$$

$$C_2 = \left(\frac{1 - \upsilon_p^2}{E_p} \right) + \left(\frac{1 - \upsilon_h^2}{E_h} \right) \tag{5}$$

Sphere-in-a-Cylinder Pivot

A spherical pivot riding in a cylindrical housing is shown in Figure 6. This pivot represents another self-aligning journal pad-pivot arrangement. Normally, both pad and housing are manufactured from carbon steel.

The deflection for this complex surface may be approximated by averaging the deflections for a spherical pivot and a sphere on a flat plate pivot [2].

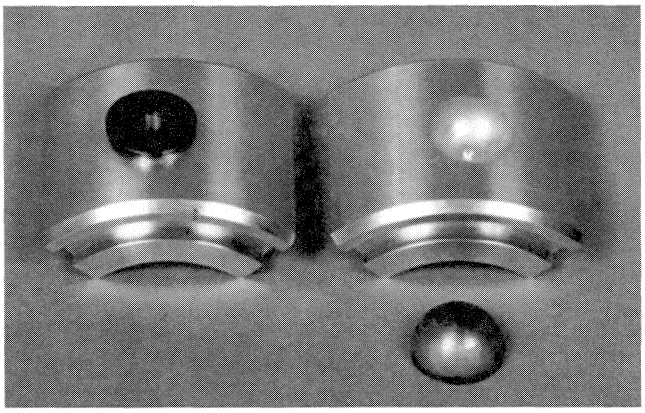

Figure 4. Bronze Pads with Steel Spherical Pivots.

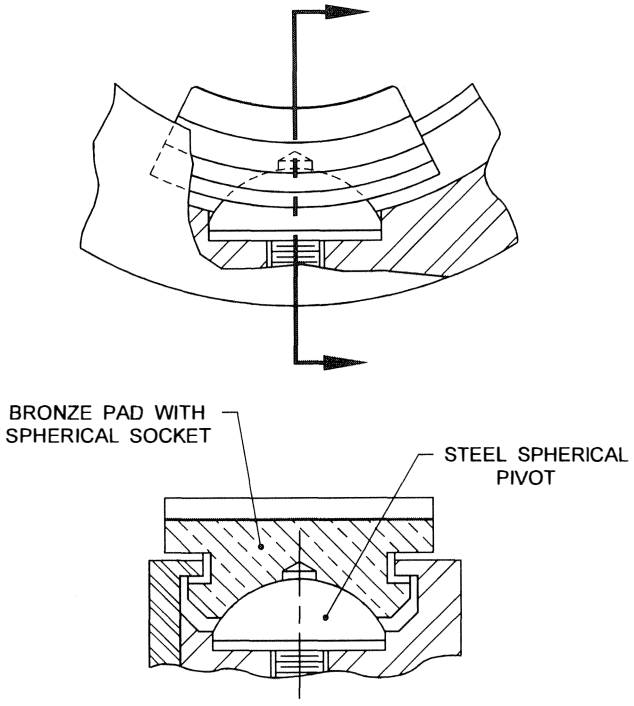

Figure 5. Steel-On-Bronze Spherical Pivot.

$$\delta_p = (.52) \cdot \left(W_p^2 C_2^2\right)^{\frac{1}{3}} \left[\frac{1}{D_p} + \frac{1}{C_1}\right]^{\frac{1}{3}} \tag{6}$$

Using Equation (1), the pivot stiffness can be determined.

$$K_p = (2.885) \cdot \left[\left(\frac{D_p C_1}{D_p + C_1}\right)\frac{W_p}{C_2^2}\right]^{\frac{1}{3}} \tag{7}$$

Cylindrical Pivot

A cylindrical pivot riding in a cylindrical housing is illustrated in Figure 7. This pivot is typical of a nonaligning journal pad-pivot arrangement. For a pivot and housing of the same material (usually, carbon steel), the elastic modulus, E, and Poissons ratio, υ, are:

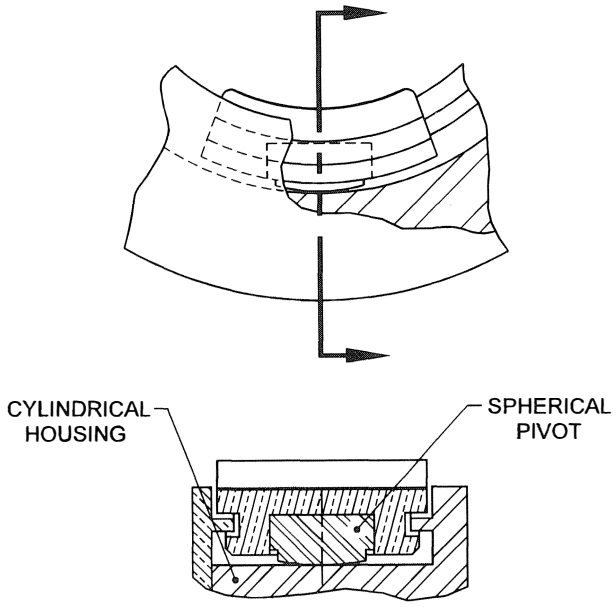

Figure 6. Steel Sphere in a Steel Cylinder Pivot.

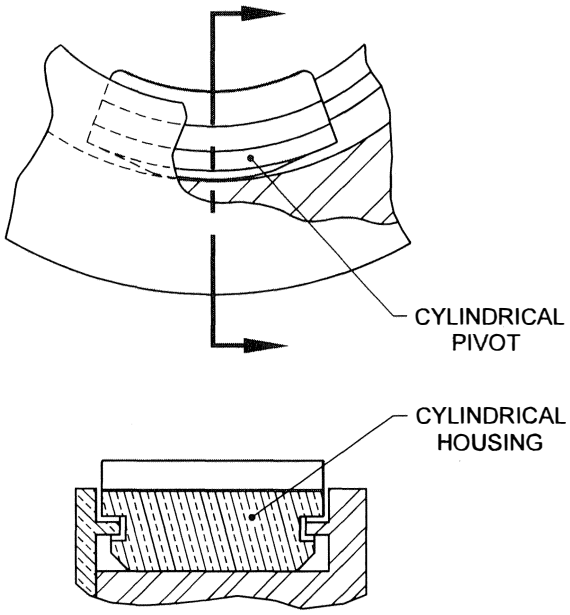

Figure 7. Steel-On-Steel Cylindrical Pivot

$$\begin{aligned} E &= E_p = E_h \text{ (psi)} \\ \upsilon &= \upsilon_p = \upsilon_h \end{aligned} \tag{8}$$

The pivot deflection is [2, 5]

$$\delta_p = \frac{2W_p(1-\upsilon^2)}{\pi L_p E}\left[\frac{2}{3} + \ln\left(\frac{2D_h}{b}\right) + \ln\left(\frac{2D_p}{b}\right)\right] \tag{9}$$

where

$$b = 2.15\sqrt{\frac{W_p D_h D_p}{L_p E(D_h - D_p)}} \tag{10}$$

For a steel pivot and housing

$$\upsilon_p = \upsilon_h = 0.3$$
$$E = 30.0\times10^6 \text{ (psi)} \tag{11}$$

The pivot stiffness is [2]

$$K_p = L_p\left\{1.93\times10^{-8}\left[16.74 + \ln\left(\frac{L_p(D_h - D_p)}{W_p}\right)\right]\right\} \tag{12}$$

DIFFERENTIAL DIAMETER AND DIFFERENTIAL THERMAL GROWTH

From Equations (3), (4), (7), and (12), clearly the pivot stiffness is a function of the diameter of the pivot and the diameter of the housing at operating temperatures. Specifically, the differential diameter, ΔD, has a strong influence on the pivot stiffness. The closer these two diameters are to each other, the higher the pivot stiffness.

Usually, the housing diameter, D_h, is slightly larger than the pivot diameter, D_p. For cylindrical and sphere-in-a-cylinder pivots, these diameters are set in the pivot design process. Furthermore, the differential diameter changes very little from ambient temperatures to operating temperatures since usually the pivot and housing materials are nearly the same (carbon steel). For these cases, since the differential thermal growth is negligible, the differential diameter is simply the difference in the housing and pivot diameters at ambient temperatures.

$$\Delta D = D_h - D_p \text{ (in)} \tag{13}$$

For spherical pivots, normally the pivot is made from carbon steel and the tilting pad, where the spherical housing is located, is manufactured from bronze. Now, the differential diameter changes from ambient to operating temperature and can significantly alter the pivot stiffness. Assuming that the pad and pivot temperatures are the same and ΔT is the temperature rise from ambient to operation, the differential thermal growth is

$$\Delta D_t = (\mu_h - \mu_p)\cdot\Delta T\cdot D_p \text{ (in)} \tag{14}$$

For a carbon steel pivot and a bronze pad (housing), the coefficients of thermal expansion, μ, are approximately:

$$\mu_p = 6.8\times10^{-6} \text{ in/in° F}$$
$$\mu_h = 10.0\times10^{-6} \text{ in/in° F} \tag{15}$$

A plot of the differential thermal growth for steel-on-bronze spherical pivots of various pivot diameters is shown in Figure 8. Clearly, as the pivot diameter, D_p, increases and as ΔT increases, the differential thermal growth increases. For example, for D_p = 2.0 in and ΔT = 100°F, ΔD = 0.64 mil whereas for D_p = 4.0 in and ΔT = 150°F, ΔD = 1.92 mil.

Thus, for steel-on-bronze spherical pivots, the differential diameter is the difference in the housing and pivot diameters at ambient temperatures plus the differential thermal growth.

$$\Delta D = \Delta D_t + (D_h - D_p) \text{ (in)} \tag{16}$$

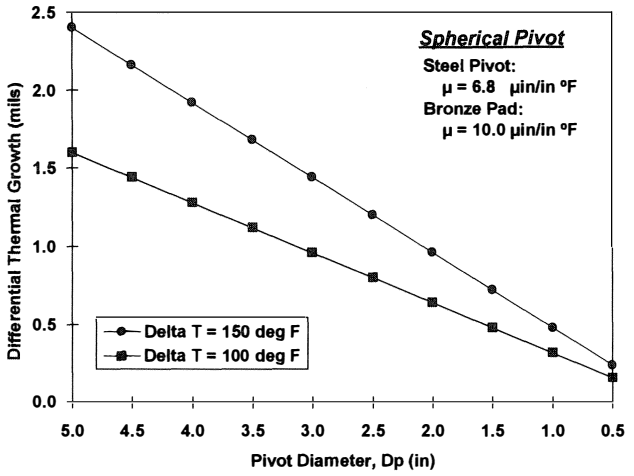

Figure 8. Steel-On-Bronze Spherical Pivot Differential Thermal Growth, ΔD_t.

The effect on pivot stiffness of differential diameter is shown in Figure 9 for steel-on-bronze spherical pivots of various pivot diameters. As the differential diameter increases, the pivot stiffness decreases. This is also true for decreasing the pivot diameter. Over-plotted on Figure 9 is a line that corresponds to the calculated differential diameter from Equations (14, 15, and 16) for ΔT = 100°F and assuming that the spherical pivot is in line-to-line contact at ambient temperature (i.e., $D_h = D_p$). For these cases, the pivot stiffness ranges from about 18.0 to 30.0 × 10^6 lb/in.

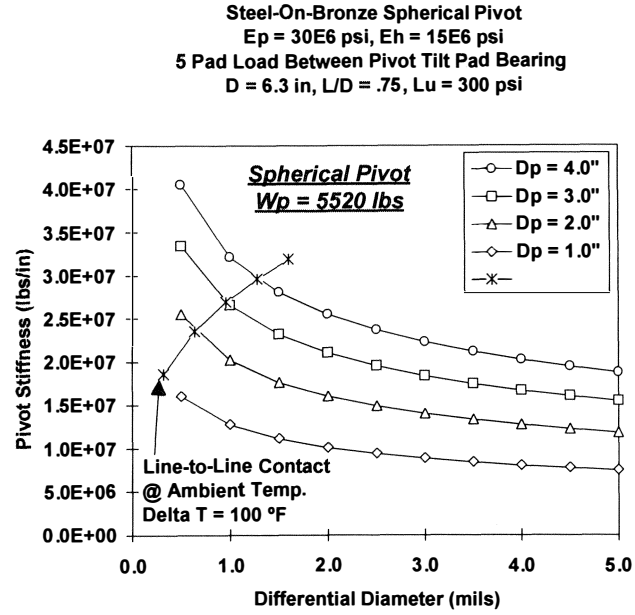

Figure 9. Steel-On-Bronze Spherical Pivot Stiffness vs Differential Diameter, ΔD, for Various Pivot Diameters.

A comparison of pivot stiffness as a function of differential diameter is illustrated in Figure 10 for a steel-on-bronze spherical pivot, a steel-on-steel cylindrical pivot and a steel sphere in a steel cylinder pivot. Generally, the spherical and cylindrical pivots produce the same high pivot stiffness values that range above 20.0 × 10^6 lb/in, whereas, the sphere-in-a-cylinder pivot

produces relatively low pivot stiffnesses that range below 7.0 × 10^6 lb/in.

All pivots shown in Figures 9 and 10 are representative of pivot designs for a five pad tilting pad bearing with a journal diameter of D = 6.3 in, a pad length of L = 4.725 in and a unit loading of L_u = 300 psi. For a five pad bearing with between pivot loading, the pivot load, W_p may be calculated:

$$W_p = \frac{L_u \cdot L \cdot D}{2 \cdot \cos(36°)} \quad (17)$$

This results in a pivot load of W_p = 5520 lb on the loaded pivots.

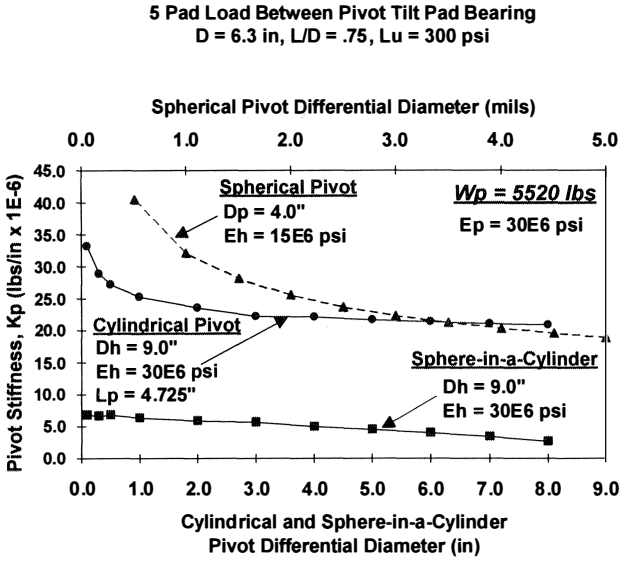

Figure 10. Pivot Stiffness vs *Differential Diameter, ΔD, for Spherical, Cylindrical and Sphere-in-a-Cylinder Pivots.*

EQUIVALENT STIFFNESS AND DAMPING

Since the pivot flexibility is inline or in series with the oil film's stiffness and damping properties, a low pivot stiffness results in a reduction or degradation in these properties. This reduction in stiffness may result in lowering a rotor's lateral critical speed into the operating speed range while a reduction in damping would increase rotor vibration for a given amount of unbalance. The same effect occurs with the introduction of a support or casing flexibility [3, 4].

If the tilting pad, pivot, and support are infinitely stiff, the rotor experiences the bearing's oil film stiffness and damping properties directly. With a flexible pivot behind the oil film, these two flexibilities, oil film and pivot, act in series to produce an equivalent stiffness and damping that are in general lower that the bearing's original properties. Now, the rotor experiences these equivalent coefficients and not the higher bearing coefficients. The model utilized in combining the oil film flexibility with the pivot stiffness is illustrated in Figures 11 and 12. Since each pad contains a pivot, the single pad oil film stiffness, K_d, and single pad oil film damping, C_d, are combined with the pad's pivot stiffness, K_p, according to Equations (A-8, A-9, A-10, A-11, and A-12) derived in the APPENDIX. Pivot damping and pad mass are also included but are usually neglected. This results in the equivalent stiffness, K_{eq}, and equivalent damping, C_{eq}, for the single pad. Next, the equivalent stiffness and damping contributions from each pad are assembled [6, 7] to obtain

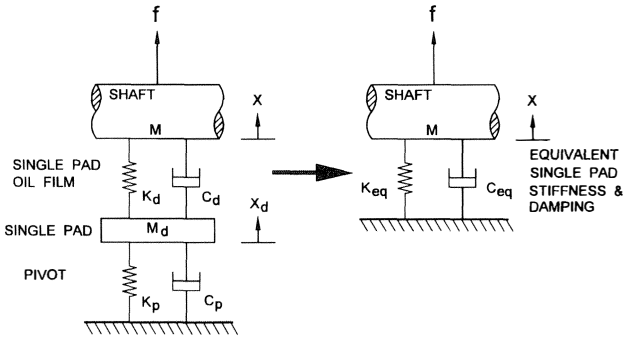

Figure 11. Equivalent Single Pad Stiffness and Damping Model.

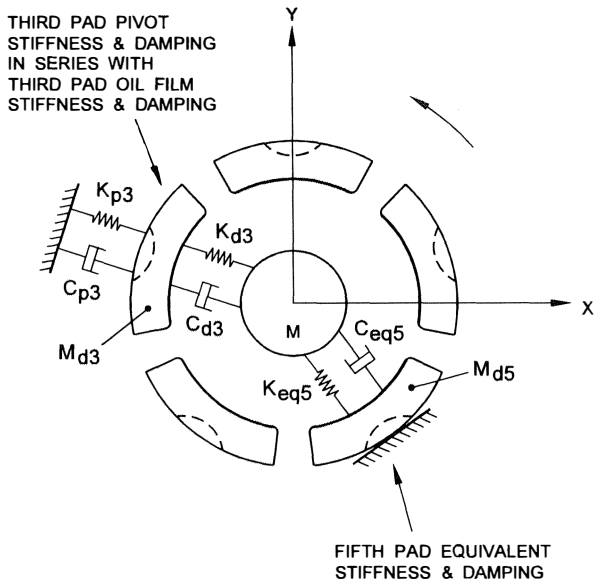

Figure 12. Equivalent Stiffness and Damping Model for Third and Fifth Pads.

the equivalent properties of the entire tilting pad bearing, K_{exx}, K_{eyy}, C_{exx}, and C_{eyy}.

The effect of pivot flexibility on the equivalent bearing stiffness is illustrated in Figure 13. In the pivot stiffness range that includes steel-on-bronze spherical pivots and steel-on-steel cylindrical pivots (i.e., K_p = 20.0 to 30.0 × 10^6 lb/in), the equivalent bearing stiffness remains relatively constant. Any further reduction in K_p results in a large decrease in equivalent stiffness. For example, K_{eyy} decreases from 8.0 × 10^6 lb/in in the spherical and cylindrical pivot range down to 3.5 × 10^6 lb/in in the sphere-in-a-cylinder range.

A similar set of curves for the bearing equivalent damping is shown in Figure 14. Again, the damping decreases drastically from the spherical and cylindrical pivot range compared to the sphere-in-a-cylinder range. Specifically, C_{eyy}, decreases by a factor of 5.5 from 5,500 to 1,000 lb-s/in (an 82 percent decrease).

HERTZIAN CONTACT PIVOT STRESS

When a pivot is loaded against a housing, point or line contact changes to area contact. It is extremely important that the resulting Hertzian contact stress does not cause a surface failure. The following equations from Shigley and Mitchell (pp. 85-87) [8], may be used to calculate the radius of contact, contact depth and maximum stress that result from pivot loading.

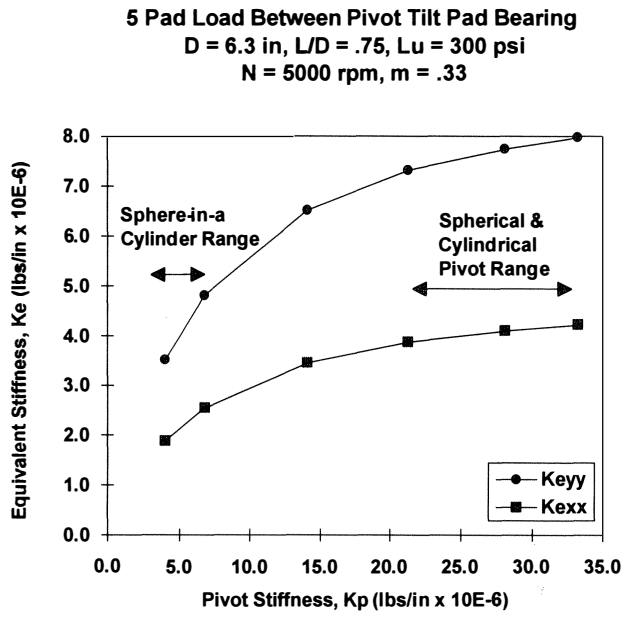

Figure 13. Equivalent Bearing Stiffness, K_e, vs Pivot Stiffness, K_p.

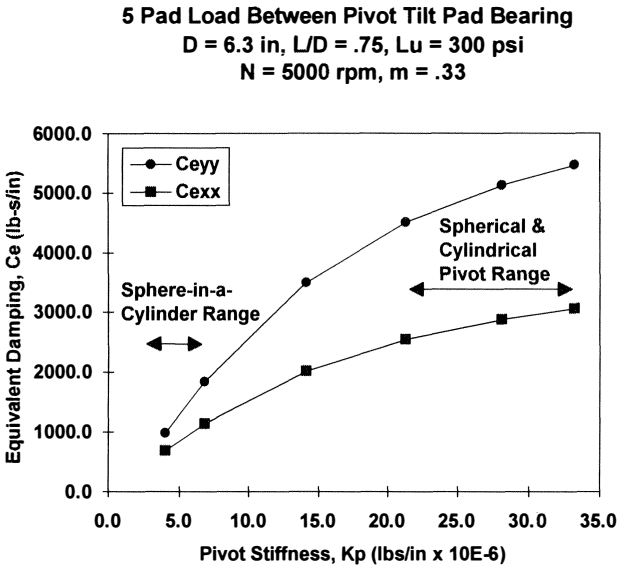

Figure 14. Equivalent Bearing Damping, C_e, vs Pivot Stiffness, K_p.

Spherical Pivots

Consider a spherical pivot with a pivot load of W_p. The resulting circular contact radius, a, is (Figure 15).

$$a = \left(\frac{3W_p C_1 C_2}{8} \right)^{\frac{1}{3}} \tag{18}$$

This results in a contact depth, h, of

$$h = R_p - \sqrt{R_p^2 - a^2} \tag{19}$$

or

$$a = \sqrt{h \cdot (2R_p - h)} \tag{20}$$

and a contact area of

$$A = 2\pi h R_p \tag{21}$$

where C_1 and C_2 are given by equaitons (4) and (5).

The corresponding maximum stress, σ_m, is

$$\sigma_m = \frac{3W_p}{2\pi a^2} \text{ (psi)} \tag{22}$$

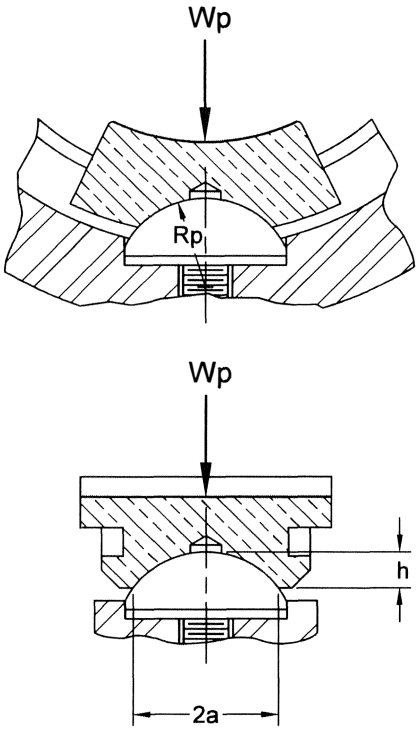

Figure 15. Spherical Pivot Schematic for Pivot Stress—Full Contact Pivot.

Cylindrical Pivots

Consider a cylindrical pivot with a pivot load of W_p. The resulting rectangular contact half-width, d, is:

$$d = \left(\frac{3W_p C_1 C_2}{\pi L_p} \right)^{\frac{1}{2}} \tag{23}$$

The corresponding maximum stress is

$$\sigma_m = \frac{2W_p}{\pi d L_p} \tag{24}$$

Sphere-in-a-Cylinder Pivot

For a sphere on a flat plate, set $C_1 = D_p$ and use Equations (18, 19, 20, 21, 22). As before with the pivot stiffness, the stress for a sphere-in-a-cylinder pivot may be approximated by averaging the stress for a spherical pivot and the stress for a sphere on a flat plate.

PIVOT WEAR AND BEARING CLEARANCE CONSIDERATIONS

High Hertzian contact stress results from high static and/or high dynamic loads on the bearing's tilting pads and thus the pad pivots. For poorly designed pivots, these high stresses may result in the spherical pivot failure shown in Figures 1 through 3. Poorly designed steel-on-steel cylindrical pivots often experience local yielding on the pad's outside diameter, which acts as the pad's pivot, and on the housing inside diameter [9]. This brinelling damage is shown in Figure 16 where both the pad and housing wear is clearly noticeable.

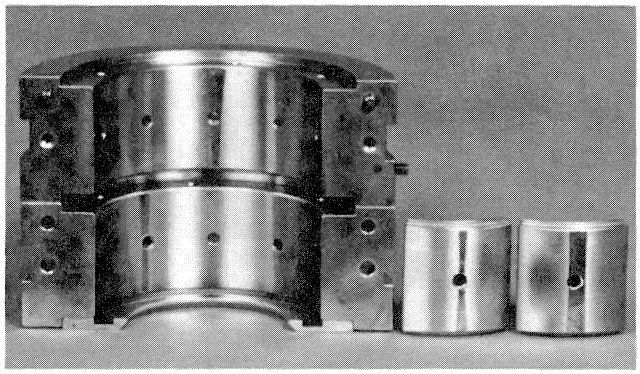

Figure 16. Steel-on-Steel Cylindrical Pivot—Housing and Pad Pivot Wear.

This wear results in the bearing clearance increasing with operation. As the clearance increases, the bearing damping decreases causing the rotor vibration to increase. This in turn increases the dynamic load on the pivot causing increased wear.

This effect of increased bearing clearance on the bearing's equivalent stiffness and damping properties is illustrated in Figures 17 and 18. Bearing stiffness and damping both decrease drastically as bearing clearance increases. As the bearing diametral clearance increases from 7.5 to 18.0 mil, the bearing's horizontal equivalent stiffness changes from 4.6×10^6 to 2.0×10^6 lb/in, a decrease of 57 percent. Similarly, the bearing's vertical equivalent stiffness changes from 8.7×10^6 to 4.0×10^6 lb/in, a decrease of 54 percent. The bearing's effective damping also changes from 4.7×10^3 to 1.3×10^3 lb-s/in horizontally, a 72 percent decrease, and from 7.8×10^3 to 2.6×10^3 lb-s/in vertically, a 67 percent decrease. For this bearing with a 6.3 in bore, a normal design clearance is about 9.5 to 12.5 mil diametral (1.5 to 2.0 mil of diametral clearance per inch of journal diameter).

SPHERICAL PIVOT HERTZIAN CONTACT STRESS, CONTACT RADIUS, AND CONTACT DEPTH

Spherical pivots of various sizes and designs are illustrated in Figure 19. The size ranges from $D_p = 0.5$ to 5.0 in. Some of the pivots are nearly half-balls while others are considerably thinner. Examples of these thin, low profile pivots may be seen in the top row of Figure 19. The thin profile is necessary to maintain a minimum of pivot intrusion into the back of the pad especially for the larger size pivot diameters (above $D_p = 1.0$ in). The pivot

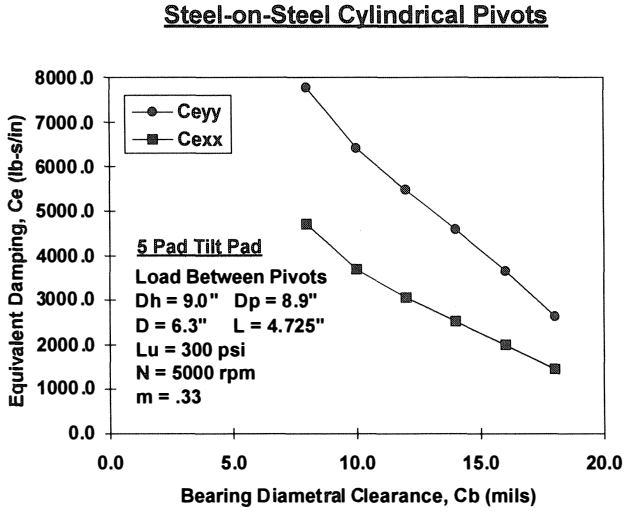

Figure 17. Equivalent Bearing Stiffness, K_e, vs Bearing Clearance.

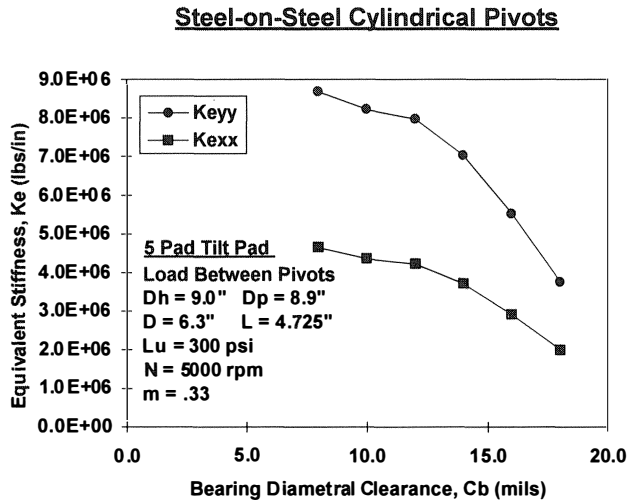

Figure 18. Equivalent Bearing Damping, C_e, vs Bearing Clearance.

intrusion into the pad is simply the depth of the spherical socket machined into the back of the tilting pad (Figure 20).

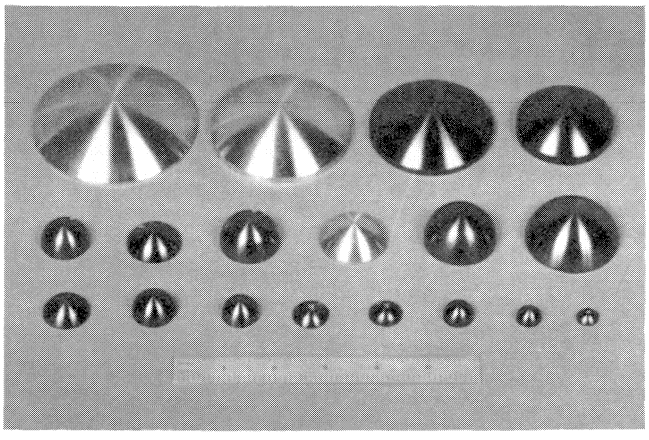

Figure 19. Steel Spherical Pivots of Various Sizes.

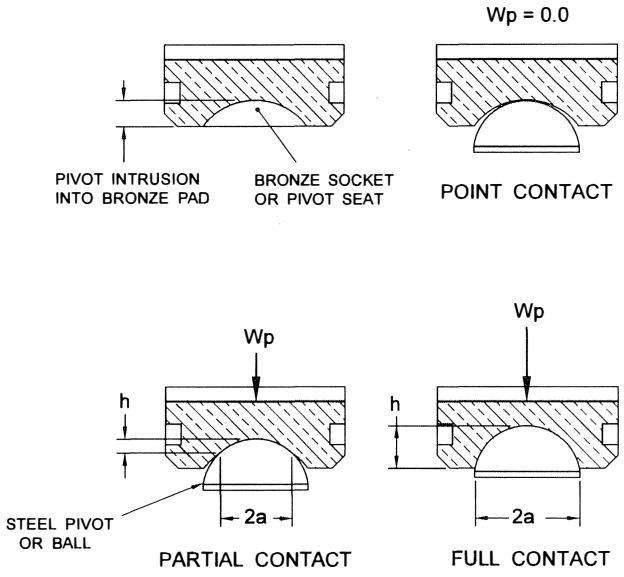

Figure 20. Spherical Pivot Contact Radius, a, and Contact Depth, h.

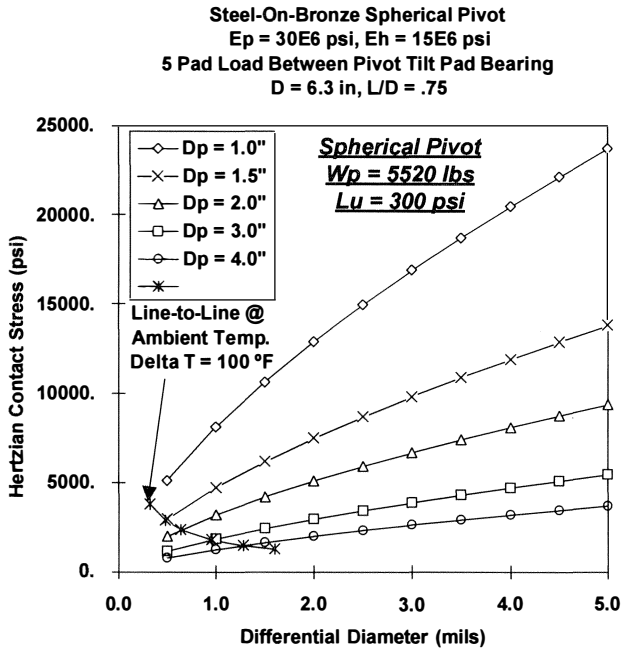

Figure 21. Steel-on-Bronze Spherical Pivot Contact Stress—L_u = 300 psi Unit Load.

Pivot contact radius is the radius of contact between the spherical ball pivot and the spherical seat in the pad. For steel-on-bronze spherical pivots, the differential thermal growth causes the bronze spherical seat in the pad to grow slightly larger compared to the steel pivot. For zero pivot load, the steel pivot is in point contact with the bronze seat in the pad (Figure 20).

As load is applied, the elastic properties of the bronze allow the seat to conform or contact the steel pivot over a portion of the pivot, as shown in Figure 20. Finally, for large enough pivot loads, full contact is established, as shown in Figure 20. The radius of this contact is defined as the pivot contact radius, a. The contact depth, h, which is also illustrated in Figure 20, is defined as the depth of contact between the steel ball and the spherical seat. A full contact pivot is also shown in Figure 15.

As long as the resulting pivot stresses do not exceed the yield stress of the bronze pad, the elastic deformation of the bronze socket will return to its original profile as the pivot load is reduced. However, when the yield stress is exceeded, plastic deformation occurs and the contact deformation becomes permanent. As the load increases further past the ultimate stress, a pivot failure occurs similar to the cracked and broken pads shown in Figures 1 through 3.

Using Equations (18, 19, 20, 21, and 22), the Hertzian contact stress, the contact radius and contact depth may be calculated for steel-on-bronze spherical pivots of various pivot diameters. These results may be seen as a function of differential pivot diameter in Figures 21, 22, 23, 24, 25, and 26.

Contact stress verses differential diameter for pivot diameters that range from D_p = 1.0 to 4.0 in is illustrated in Figure 21 for a five pad load between pivot bearing with an L_u = 300 psi unit load. Similar results are presented in Figure 22 for a unit load of 500 psi. The line showing the differential diameter that results from line-to-line contact at ambient temperature is over-plotted on the curves.

From the results for both the 300 and 500 psi unit load cases (Figures 21 and 22), the pivot stresses range below 5000 psi for all pivot diameters with line-to-line contact at ambient temperature. Since the yield stress for the bronze pad is σ_y = 18 ksi, the contact stresses are below σ_y for bronze for all pivot diameters whose differential diameter ranges up to 5.0 mil except the D_p =

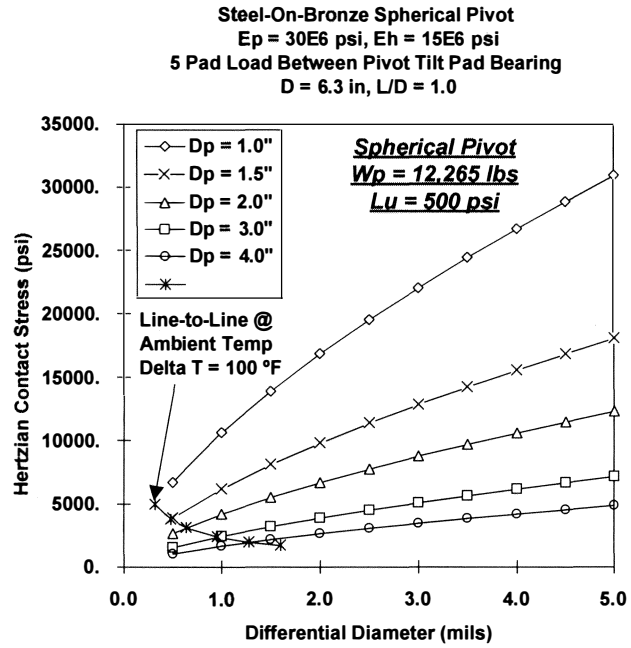

Figure 22. Steel-on-Bronze Spherical Pivot Contact Stress—L_u = 500 psi Unit Load.

1.0 in pivot. However, these results are misleading, since the pivot contact radius and contact depth must also be examined.

The pivot contact radius for the 500 psi unit loading case is shown in Figure 23. Consider the D_p = 1.0 in pivot. The calculated contact radius ranges up to 0.9 in. However, the maximum contact radius is limited by the physical size of the pivot. Clearly, the contact radius can never be larger than the actual pivot radius ($a \leq R_p$). This maximum contact radius line is also shown in Figure 23.

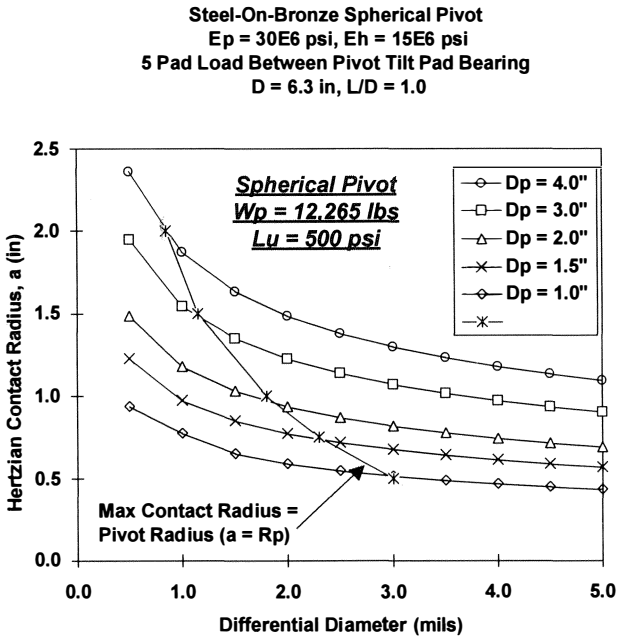

Figure 23. Steel-on-Bronze Spherical Pivot Contact Radius.

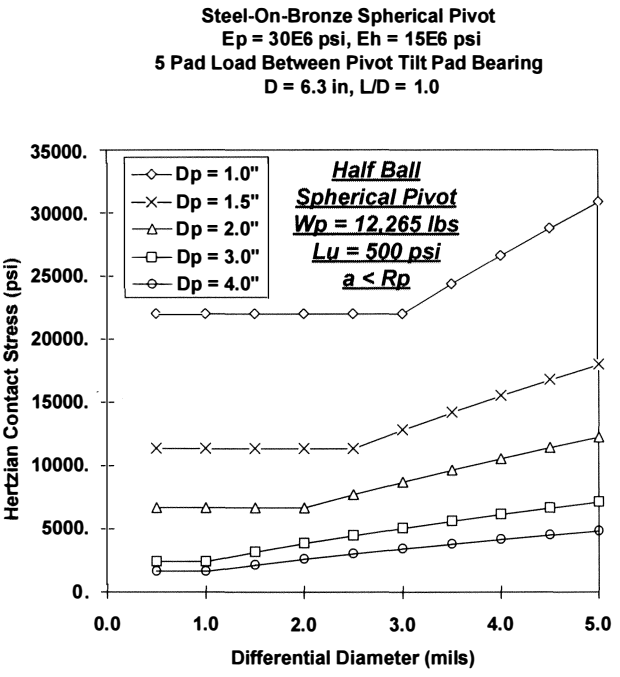

Figure 24. Steel-on-Bronze Half Ball Spherical Pivot Stress—Maximum Contact Radius = Pivot Radius (a = R_p).

Thus, for any contact radius that exceeds R_p, set a = R_p, and replot Figure 22. These results are shown in Figure 24. Now, contact stresses are considerably larger compared to Figure 22 for differential diameters under 3.0 mil. Full half-ball pivots (i.e., pivots whose height = R_p) are represented in Figure 24. However, when pad thickness is considered, these results may still be misleading as contact depth must also be examined.

The corresponding contact depth is shown in Figure 25 for the 500 psi unit load case. Note that for low values of differential diameter, the contact depth ranges up to 1.3 in. This may be

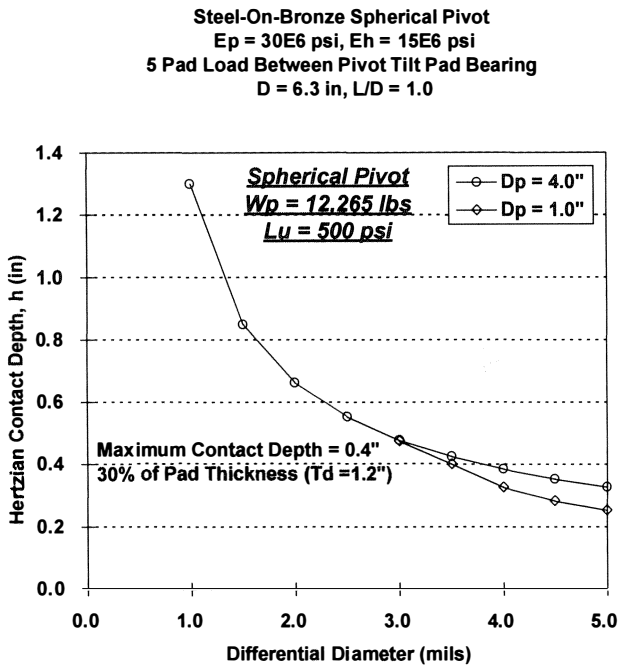

Figure 25. Steel-on-Bronze Spherical Pivot Contact Depth.

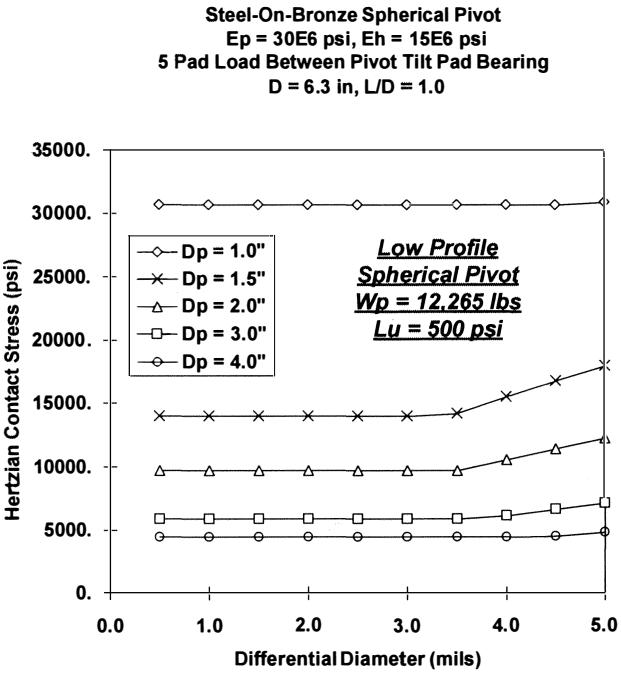

Figure 26. Steel-on-Bronze Spherical Pivot Contact Stress—Low Profile Pivots.

physically unreasonable if the pad thickness is limited by geometric considerations. For this five pad bearing example, the journal diameter is D = 6.3 in. A reasonable pad thickness is T_d = 1.2 in. Good pad design practice allows the pivot intrusion to be about 30 percent of the pad thickness. Thus, the maximum contact depth for this example is h = 0.4 in. In this case, a low profile pivot must be used where the pivot height is considerably less than R_p.

Thus, for any contact depth that exceeds 0.4 in, set h = 0.4 and replot Figure 24. Now, a much more reasonable representation of the contact stresses for the example pivot is shown in Figure 26. Again, the contact stresses are considerably larger for differential diameters less than 3.5 mil compared to Figure 24. In fact, pivot diameters less than 2.0 in may be eliminated from consideration as they result in contact stresses that exceed or are too close to σ_y = 18 ksi for bronze.

SPHERICAL PIVOT DESIGN PROCEDURE

In order to demonstrate a pivot design procedure for high load applications, a specific example of an actual industrial application will be instructive. Consider the following application for a five pad tilting pad bearing with steel-on-bronze spherical pivots for an integrally geared compressor (Figure 27). Since the pad thickness is limited by geometric considerations to T_d = 1.2 in, low profile pivots will be considered.

Journal diameter, D	=	6.3 in
Pad length, L	=	6.3 in
Pad thickness, T_d	=	1.2 in
Total resultant bearing load, W_b	=	19,845 lbs
Unit load, L_u	=	500 psi

Assume the following material properties:

Steel pivot:	E_p	= 30×10^6 psi
	ν_p	= 0.30
	μ_p	= 6.8×10^6 in/in °F
	σ_y	= 115 ksi
	σ_t	= 140 ksi
Bronze pad:	E_h	= 15×10^6 psi
	ν_h	= 0.34
	μ_h	= 10.0×10^6 in/in °F
	σ_y	= 18 ksi
	σ_t	= 35 ksi
	σ_c	= 46 ksi

In order to design conservatively, the yield stress of the bronze pad with the spherical pivot seat will be used for the design stress criterion with an appropriate safety margin as opposed to the material tensile or compressive stress.

Normally, for high load applications, the resultant load is directed between pivots and W_p = 12,265 lb. This is the example bearing considered previously in Figures 22 through 26. Again, for conservative design purposes, assume that all of the load is directed onto one single pivot. Thus,

Pivot load, W_p = 19,845 lb

First, consider a pivot diameter of D_p = 2.0 in (R_p = 1.0 in). From the pad and pivot geometry, the pivot intrusion into the back of the pad is specified as 0.36 in. Thus, the maximum contact depth possible is h = 0.36 in, which corresponds to a maximum contact radius of a = 0.77 in using Equation (20).

Assuming a 100°F temperature rise, line-to-line contact at ambient temperature and using equations (14) and (16), ΔD = 0.6 mil. Thus, at operating conditions, assume D_p = 2.0000 and D_h = 2.0006 in.

From Equations (2, 3, 4, and 5),

Pivot deflection, δ_p = 0.8 mil

Pivot stiffness, K_p = 36.8 × 10^6 lb/in

From Equation (18), the contact radius is a = 1.6 in. This is considerably larger than the maximum allowable of 0.77 in. Using a = 0.77 in and Equation (22),

Contact stress, σ_m = 15,980 psi

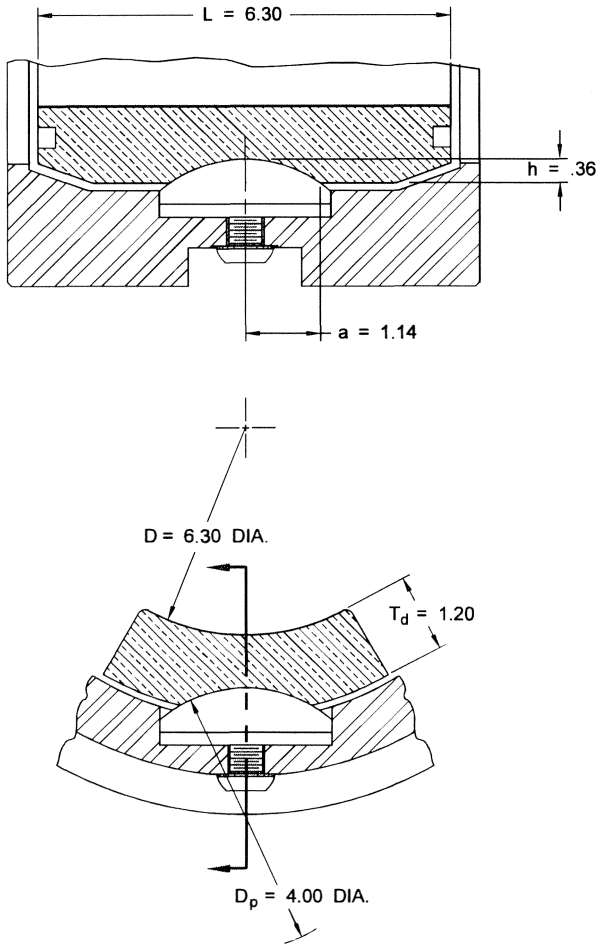

Figure 27. Example D_p = 4.0 Inch Low Profile Spherical Pivot.

Since σ_m very nearly exceeds σ_y, consider a larger pivot diameter of D_p = 3.0 in. Again, from the pad and pivot geometry, the pivot intrusion into the back of the pad is 0.36 in. Thus, the maximum contact depth possible is 0.36 in, which corresponds to a maximum contact radius of 1.0 in using Equation (20).

Assuming a 100°F temperature rise, line-to-line contact at ambient temperature and using Equations (14) and (16), ΔD = 1.0 mil. Thus, at operating conditions, assume D_p = 3.000 and D_h = 3.001 in. Thus,

Pivot deflection, δ_p = 0.7 mil

Pivot stiffness, K_p = 40.6 × 10^6 lb/in

From Equation (18), the contact radius is a = 1.8 in. This is considerably larger than the maximum allowable of 1.0 in. Using a = 1.0 in and Equation (22),

Contact stress, σ_m = 9,475 psi

Now, σ_m is less than σ_y by 47 percent and the D_p = 3.0 in pivot appears to be satisfactory. However, the above calculations most nearly approximate the static stress levels (i.e., the pivot stress for zero dynamic load). Since nearly all rotors vibrate, a dynamic load exists and should be included in the pivot stress calculation.

To estimate the dynamic load for a rotor, the following equation may be used:

$$F_n = \frac{W}{g} \cdot \left(\frac{TIR}{2}\right) \cdot \left(\frac{N\pi}{30}\right)^2 \qquad (25)$$

Consider the force caused by the unbalance from 4.0 mil of total indicator reading (TIR) runout for a 200 lb rotor running at 20,000 rpm. From the above equation, F_d = 4,546 lb. Also, a 900 lb rotor running at 9,000 rpm produces a dynamic force of 4,142 lb.

Thus, assuming a dynamic load of 5,000 lb for this example, the total pivot load becomes W_p = static + dynamic = 19,845 + 5000 = 24,845 lb. Now, for the D_p = 3.0 in pivot, the contact stress becomes σ_m = 11,860 psi which is 34 percent below the yield stress for the bronze pad.

In order to increase the safety factor, consider a 4.0 in pivot. From the pad and pivot geometry, the pivot intrusion into the back of the pad is again 0.36 in (Figure 27). Thus, the maximum contact depth possible is 0.36 in, which corresponds to a maximum contact radius of 1.14 in.

Assuming a 100°F temperature rise, line-to-line contact at ambient temperature and using Equations (14) and (16), ΔD = 1.3 mil. Thus, at operating conditions, assume D_p = 4.0000 and D_h = 4.0015 in. With W_p = 24,845 lb,

Pivot deflection, δ_p = 0.8 mil

Pivot stiffness, $K_p = 46.4 \times 10^6$ lb/in

From Equation (18), the contact radius is a = 2.1 in. This is considerably larger than the maximum allowable of 1.14 in. Using a = 1.14 in and Equation (22),

Contact stress, σ_m = 9,128 psi

This is 49 percent below the yield stress of bronze. These results are listed in Table 1.

Table 1. Summary of Example Steel-on-Bronze Pivot Stiffness and Stress Calculations.

D_p (in)	ΔD (in)+	a (in)	W_p (lbs)	δ_p (mils)	K_p (lbs/in)	σ_m (psi)	Margin++
2.0	0.6	0.77	19,845*	0.8	36.8×10^6	15,980	11%
3.0	1.0	1.0	19,845*	0.7	40.6×10^6	9,475	47%
4.0	1.5	1.14	19,845*	0.7	43.0×10^6	7,291	59%
3.0	1.0	1.0	24,845**	0.9	43.8×10^6	11,860	34%
4.0	1.5	1.14	24,845**	0.8	46.4×10^6	9,128	49%

\+ Assumes line-to-line contact at ambient and a 100°F temperature rise.
++ Safety margin of σ_m below yield stress, σ_y.
* Static resultant load only.
** Static + dynamic load.

FINITE ELEMENT STRESS ANALYSIS

In an effort to determine the validity of using the simple equations to calculate the maximum contact stress for spherical pivots, a finite element stress analysis is performed. A representation of the three dimensional finite element model for the example bronze pad and steel pivot from the last section is illustrated in Figure 28. Because of symmetry, only 1/4 of the pad and pivot is considered. The pivot diameter is 4.0 in and the differential diameter is 1.5 mil. The model consists of 196 three dimensional brick elements. Nonlinear gap elements are used between the pad's spherical socket and ball pivot. The steel ball pivot is assumed to be rigid.

The load profile is assumed to be parabolic in the axial and circumferential directions. Forces are applied to the pad surface at discreet nodal locations as shown in Figure 28. The total load for 1/4 of the pad is set equal to 25 percent of the pivot load, W_p.

Finite element stress contour plots of maximum principal stress are presented in Figures 29 and 30 for pivot loads of 19,845 lb and 24,845 lb, respectively. Note that the maximum pivot compressive stress area is at the center of the spherical seat in the pad. This corresponds to the area of cracking from the spherical pivot failure shown in Figure 1.

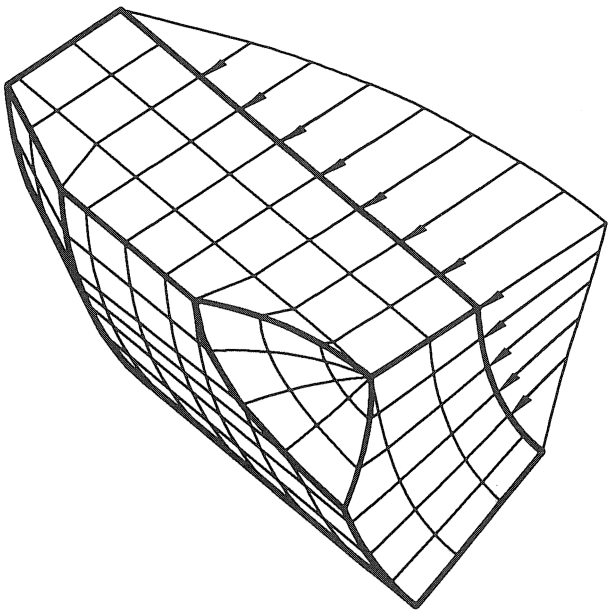

Figure 28. Steel-on-Bronze Spherical Pivot Finite Element Model Representation, D_p = 4.0 Inch, ΔD = 1.5 Mil.

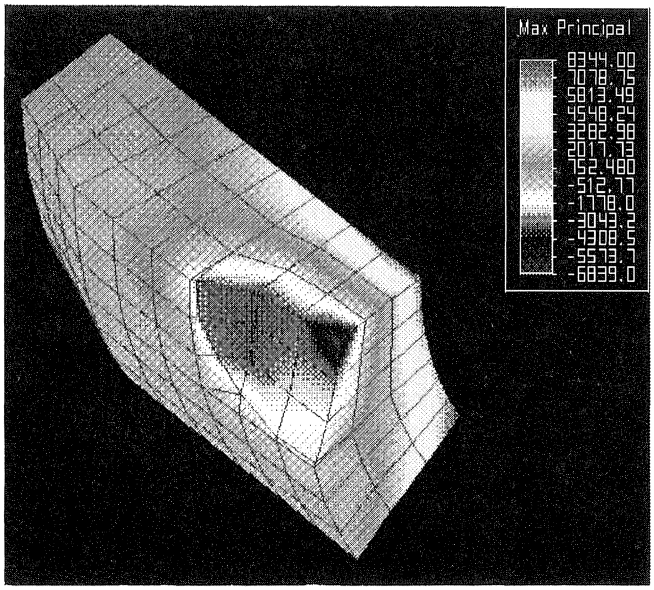

Figure 29. Steel-on-Bronze Spherical Pivot Finite Element Stress Contours, D_p = 4.0 Inch, ΔD = 1.5 Mil, W_p = 19,845 Lb.

A summary of the maximum principal stress from the finite element analysis and the maximum Hertzian contact stress calculated with the simplified equations are listed in Table 2. Note that the stress results are in general agreement. The finite element stress values are slightly lower than the simplified equation results.

FRICTIONAL MOMENT

One disadvantage of spherical pivots is that the bronze spherical seat in the tilting pad does not actually pivot on the steel ball but, instead, it slides. The resultant bearing load applies a normal force on each pivot which in turn creates a frictional

Table 2. Comparison of Example Steel-on-Bronze Pivot Stress—Simple Equations vs *Finite Element Solution.*

W_p (lbs)	D_p (in)	ΔD (in)	Simple Equations σ_m (psi)	Finite Elements σ_m (psi)
19,845	4.0	1.5	7,291	6,839
24,845	4.0	1.5	9,128	7,149

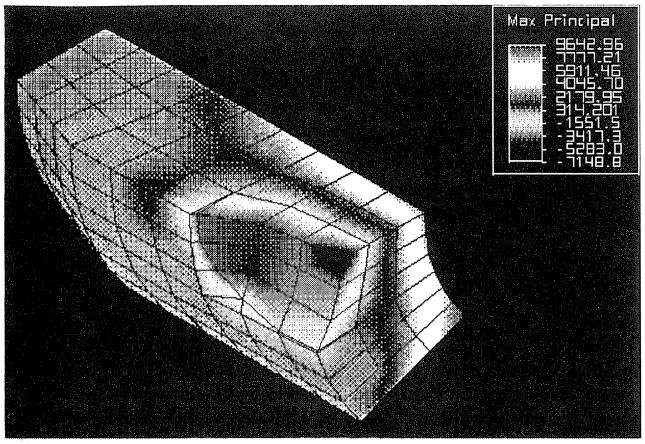

Figure 30. Steel-on-Bronze Spherical Pivot Finite Element Stress Contours, D_p = 4.0 Inch, ΔD = 1.5 Mil, W_p = 24,845 Lb.

moment that resists the pad's ability to tilt. This is illustrated in Figure 31 where, for simplicity, a point contact is assumed.

Since the pad tilts about the pivot's center, consider a moment summation about "o." The dynamic force due to unbalance rotates around the bearing once per revolution. As this force moves along the circumferential length of the pad, the pad wants to tilt to accommodate the dynamic force. The pad will not tilt until the dynamic force moment, M_n, exceeds the frictional moment, M_f. Thus, for the pad to tilt,

$$M_n > M_f$$

$$[F_{nx} \cdot (R_p + \ell_2)] + (F_{ny} \cdot \ell_1) > (F_f \cdot R_p)$$

For a given pivot load, W_p, the normal force and thus the friction force, F_f, remain the same regardless of pivot diameter. The frictional moment, however, increases as the pivot radius, R_p, increases. While the dynamic moment also increases with R_p, the x direction component of the dynamic force, F_{nx}, is normally smaller than F_{ny}. Thus, pivots that are too large may prevent the pad from tilting during a dynamic excitation.

This problem is intensified for gear boxes and integrally geared compressors. For gear driven or nongear driven rotors, the dynamic force is normally of the same order of magnitude as the gravity load, the pivot load and, thus, the friction force. However, for gear driven rotors, the resultant load on the bearing may be an order of magnitude larger than the gravity load. This translates to extremely large pivot loads, normal loads and frictional moments. Thus, for rotors with large gear loads or other external nongravity loads, the friction force will be considerably larger than the dynamic force.

For a partial or full contact pivot, a good approximation is to assume that the normal force from the pivot load is distributed evenly around the spherical pivot. Now, the frictional moment becomes the summation of all frictional moment contributions from each discreet load point.

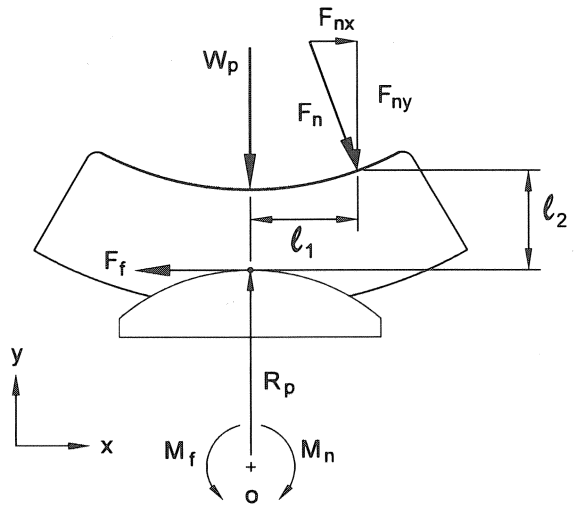

$$\text{Frictional Moment} = M_f = F_f \cdot R_p$$

$$\text{Dynamic Moment} = M_n = \left[F_{nx} \cdot (R_p + \ell_2)\right] + (F_{ny} \cdot \ell_1)$$

Figure 31. Spherical Pivot Frictional and Dynamic Moment for Point Contact.

CONCLUSIONS

The major conclusions concerning tilting pad journal bearing pivot design are summarized below.

- The differential thermal growth from ambient to operating temperature (100°F temperature rise) for a steel-on-bronze spherical pivot ranges from under 0.5 mil for a 1.0 in diameter pivot to 1.6 mil for a 5.0 in diameter pivot.

- For the example bearings and pivots analyzed herein, stiffness values range above 20.0×10^6 lb/in for the steel-on-bronze spherical pivots and the steel-on-steel cylindrical pivots. For the steel sphere in a steel cylinder pivot, stiffnesses range below 7.0×10^6 lb/in.

- For the example bearings and pivots considered, the equivalent bearing horizontal and vertical stiffnesses are above 4.2×10^6 and 7.3×10^6 lb/in, respectively, for the steel-on-bronze spherical pivots and the steel-on-steel cylindrical pivots. For the steel sphere in a steel cylinder pivot, equivalent bearing horizontal and vertical stiffnesses range below 2.5×10^6 and 4.8×10^6 lb/in, respectively.

- For the example bearings and pivots considered, the equivalent bearing horizontal and vertical damping values are above 2.5×10^3 and 4.4×10^3 lb-s/in, respectively, for the steel-on-bronze spherical pivots and the steel-on-steel cylindrical pivots. For the steel sphere in a steel cylinder pivot, equivalent bearing horizontal and vertical damping values range below 1.0×10^3 and 1.8×10^3 lb-s/in, respectively.

- Poorly designed steel-on-steel cylindrical pivots experience local pivot yielding on the pad's outside diameter and on the housing's inside diameter. This wear results in the bearing clearance increasing with operation. For the example steel-on-steel cylindrical pivots considered, as the bearing diametral clearance increases from 7.5 to 18.0 mil, the bearing's equivalent stiffness decreases 57 percent horizontally and 54 percent

vertically. The bearing's effective damping also decreases by 72 percent horizontally and by 67 percent vertically.

• Poorly designed steel-on-bronze spherical pivots may lead to pivot failure from excessive contact stresses. This failure may cause the tilting pad to crack or eventually break.

• For the 500 psi unit loading example analyzed herein, the steel-on-bronze spherical pivot produces maximum contact stresses that are below the yield stress of bronze for all cases analyzed with pivot diameters above 2.0 in and differential diameters below 5.0 mil.

• The finite element stress analysis produced results that are in general agreement with the stress calculations based on the simple equations presented herein.

• For all pivots considered, as differential diameter increases, pivot stiffness decreases and pivot contact stress increases.

• For the three different pivot designs considered, both the spherical and sphere-in-a-cylinder pivots are self-aligning. Furthermore, both the spherical and the cylindrical pivots provide high pivot stiffness. Finally, only the spherical pivot provides self-alignment capability, high pivot stiffness and low pivot stress.

• For all spherical pivots considered, as pivot diameter increases, pivot stiffness increases and pivot contact stress decreases.

• For all spherical pivots considered, as pivot contact radius and contact depth increase, pivot contact stress decreases.

• For spherical pivots, as pivot diameter increases, the frictional moment increases.

• Spherical pivot design guidelines are summarized below:

· Use the yield stress plus an appropriate safety margin as the design criteria.

· Use the total resultant bearing load plus an appropriate dynamic load for the pivot load.

· After a reasonable pad thickness is established, limit the pivot intrusion into the back of the pad to 30 percent of the pad thickness, if possible, but never over 50 percent.

· Line-to-line contact at room temperature is recommended for minimum pivot stress and maximum pivot stiffness.

· Calculate the contact radius and contact depth for a given pivot diameter and load. Attempt to size the pivot height and intrusion into the pad to match these calculations without violating the 30 to 50 percent intrusion guideline. If this is not possible, size the pivot to give the largest contact radius possible and use this contact radius to calculate the contact stress.

· If the resulting contact stress exceeds the material yield stress minus the appropriate safety margin, increase the pivot diameter and recalculate the contact stress.

· Once the safety margin is obtained, do not further increase the pivot diameter.

NOMENCLATURE

a	pivot contact radius (in)
A	pivot contact area (in^2)
b	see Equation (10)
C_1	see Equation (4)
C_2	see Equation (5)
C_b	bearing diametral clearance (mils)
C_d	single pad damping (lb-s/in)
C_e	equivalent bearing damping (lb-s/in)
C_{exx}, C_{eyy}	equivalent bearing horizontal, vertical damping (lb-s/in)
C_{eq}	equivalent single pad damping (lb-s/in)
C_p	pivot damping (lb-s/in)
d	rectangular contact half-width (in)
D	journal diameter (in)
D_h	housing diameter (in)
D_p	pivot diameter (in)
E	modulus of elasticity (psi)
E_h, E_p	housing, pivot modulus of elasticity (psi)
F, f	unbalance force (lbs)
F_n	dynamic force (lbs)
F_{nx}, F_{ny}	x, y direction dynamic force component (lbs)
F_f	friction force (lbs)
g	acceleration of gravity (in/s^2)
h	pivot contact depth (in)
K_d	single pad stiffness (lbs/in)
K_e	equivalent bearing stiffness (lbs/in)
K_{exx}, K_{eyy}	equivalent bearing horizontal, vertical stiffness (lbs/in)
K_{eq}	equivalent single pad stiffness (lbs/in)
K_p	pivot stiffness (lbs/in)
$\hat{K}_p$	see Equation (29)
ℓ_1	x direction distance from the dynamic force to the pivot center (in)
ℓ_2	y direction distance from the dynamic force to the pivot surface (in)
L	pad length (in)
L_p	pivot length (in)
L_u	= W_b/(L×D), bearing unit load (psi)
m	pad preload (dim)
M	shaft mass (lb-s^2/in)
M_d	pad mass (lb-s^2/in)
M_n	dynamic moment (in-lbs)
M_f	frictional moment (in-lbs)
N	journal rotational speed (rpm)
R_p	pivot radius (in)
t	time (s)
T	temperature (°F)
T_d	pad thickness (in)
TIR	total indicator reading (in)
W	total rotor weight (lbs)
W_b	total bearing resultant load (lbs)
W_p	pivot load (lbs)
x, X	shaft displacement (in)
x_d, X_d	pad displacement (in)
δ_p	pivot deflection (in)
ΔD	differential diameter (in)
ΔD_t	differential thermal growth (in)
ΔT	temperature differential (°F)
μ	coefficient of thermal expansion (in/in °F)
μ_h,μ_p	housing, pivot coefficient of thermal expansion (in/in °F)
ν	Poissons ratio (dim)

ν_h, ν_p	housing, pivot Poissons ratio (dim)
σ_c	compressive strength (psi)
σ_m	pivot Hertzian maximum contact stress (psi)
σ_t	tensile stress (psi)
σ_y	yield stress (psi)
ω	journal rotational speed (1/s)

APPENDIX

Equivalent Tilting Pad Characteristics

The model for a tilting pad oil film in series with a single pad pivot is shown in Figure 11. A full assembled bearing is modeled in Figure 12 showing the stiffness and damping contribution of each individual pads oil film in line with each pads pivot stiffness.

The oil film stiffness and damping properties for each pad may be calculated from bearing computer programs [6, 7]. Next, the pivot stiffness can be determined from the equations presented previously. Then, the following equations can be used to combine each pads oil film flexibility with each pads pivot stiffness. This results in the equivalent stiffness and damping properties for each individual pads oil film in line with each pads pivot. Finally, the equivalent stiffness and damping contributions from each pad are assembled [6, 7] to obtain the equivalent properties of the entire tilting pad bearing.

Prior to deriving the equations for each individual pads equivalent properties, define the following key terms:

K_d = single pad oil film stiffness, lbs/in
C_d = single pad oil film damping, lb · s/in
K_p = pivot stiffness, lbs/in
K_{eq} = single pad equivalent stiffness, lbs/in
C_{eq} = single pad equivalent damping, lb · s/in
M_d = pad mass, lb · s²/in
M = journal mass, lb · s²/in

From Figure 11, the equations of motion are

$$M\ddot{x} + C_d(\dot{x} - \dot{x}_d) + K_d(x - x_d) = f \qquad \text{(A-1)}$$

$$M_d\ddot{x}_d + C_p\dot{x}_d + C_d(\dot{x}_d - \dot{x}) + K_p x_d + K_d(x_d - x) = 0 \qquad \text{(A-2)}$$

Assuming synchronous forced response at frequency ω

$$x = Xe^{i\omega t} \qquad x_d = X_d e^{i\omega t} \qquad f = Fe^{i\omega t}$$

Equation (A-2) becomes

$$(\hat{K}_p + K_d + i\omega C_p + i\omega C_d)X_d = (K_d + i\omega C_d)X \qquad \text{(A-3)}$$

where

$$\hat{K}_p = K_p - M_d\omega^2 \qquad \text{(A-4)}$$

Equation (A-1) becomes

$$F = K_d X - K_d X_d + i\omega(C_d X - C_d X_d) - M\omega^2 X \qquad \text{(A-5)}$$

Solving for X_d in Equation (A-3) and substituting into equation (A-5) yields

$$F = \left[K_d - \frac{K_d^2 + i\omega C_d K_d}{\hat{K}_p + K_d + i\omega(C_p + C_d)}\right] X + i\omega\left[C_d - \frac{K_d C_d + i\omega C_d^2}{\hat{K}_p + K_d + i\omega(C_p + C_d)}\right] X - M\omega^2 X \qquad \text{(A-6)}$$

For the equivalent system

$$F = K_{eq}X + i\omega C_{eq}X - m\omega^2 X \qquad \text{(A-7)}$$

Combining (A-6) and (A-7), rationalizing and simplifying yields the equivalent system stiffness and damping properties

$$K_{eq} = \frac{\hat{K}_p K_d(\hat{K}_p + K_d) + \omega^2(K_d C_p^2 + \hat{K}_p C_d^2)}{(\hat{K}_p + K_d)^2 + \omega^2(C_p + C_d)^2} \qquad \text{(A-8)}$$

$$C_{eq} = \frac{K_d^2 C_p + \hat{K}_p^2 C_d + \omega^2 C_p C_d(C_p + C_d)}{(\hat{K}_p^2 + K_d)^2 + \omega^2(C_p + C_d)^2} \qquad \text{(A-9)}$$

Usually, the pivot damping is negligible and (A-8) and (A-9) simplify to

$$K_{eq} = \frac{\hat{K}_p K_d(\hat{K}_p + K_d) + \hat{K}_p(\omega C_d)^2}{(\hat{K}_p + K_d)^2 + (\omega C_d)^2} \qquad \text{(A-10)}$$

$$C_{eq} = \frac{\hat{K}_p^2 C_d}{(\hat{K}_p + K_d)^2 + (\omega C_d)^2} \qquad \text{(A-11)}$$

Also, for small pad mass,

$$\hat{K}_p = K_p \qquad \text{(A-12)}$$

and Equations (A-10) and (A-11) simplify further.

REFERENCES

1. Lund, J. W. and Pedersen, L. B., "The Influence of Pad Flexibility on the Dynamic Coefficients of a Tilting Pad Bearing," ASME Journal of Tribology, *109* (1), pp. 65-70 (1987).
2. Kirk, R. G. and Reedy, S. W., "Evaluation of Pivot Stiffness for Typical Tilting-Pad Journal Bearing Designs," ASME Journal of Vibration, Acoustics, Stress and Reliability in Design, *110* (2), pp. 165-171 (1988).
3. Nicholas, J. C., Whalen, J. K., and Franklin, S. F., "Improving Critical Speed Calculations Using Flexible Bearing Support FRF Compliance Data," *Proceedings of the Fifteenth Turbomachinery Symposium*, The Turbomachinery Laboratory, Texas A&M University, College Station, Texas (1986).
4. Nicholas, J. C. and Barrett, L. E., "The Effect of Bearing Support Flexibility on Critical Speed Prediction," ASLE Transactions, *29* (3), pp. 329-338 (1986).
5. Young, W. C., *Roarks Formulas for Stress and Strain, Sixth Edition*, New York, New York: McGraw Hill (1989).
6. Lund, J. W., "Spring and Damping Coefficients for the Tilting-Pad Journal Bearing," ASLE Transactions, *7* (4), pp. 342-352 (1964).

7. Nicholas, J. C., Gunter, E. J., and Allaire, P. E., "Stiffness and Damping Coefficients for the Five Pad Tilting Pad Bearing," ASLE Transactions, *22* (2), pp. 112-124 (1979).

8. Shigley, J. E. and Mitchell, L. D., *Mechanical Engineering Design, Fourth Edition,* New York, New York: McGraw Hill (1983).

9. Zeidan, F. Y. and Paquette, D. J., "Application of High Speed and High Performance Fluid Film Bearings in Rotating Machinery," *Proceedings of the Twenty-Third Turbomachinery Symposium*, The Turbomachinery Laboratory, Texas A&M University, College Station, Texas (1994).